The Halting Effect of Baroclinicity in Vortex Merging

SIMONA MASINA AND NADIA PINARDI

Istituto per lo Studio delle Metodologie Geofisiche Ambientali, CNR, Modena, Italy

(Manuscript received 7 October 1991, in final form 6 July 1992)

ABSTRACT

We study the quasigeostrophic merging dynamics of axisymmetric baroclinic vortices to understand how baroclinicity affects merging rates and the development of the nonlinear cascade of enstrophy. The initial vortices are taken to simulate closely the horizontal and vertical structure of Gulf Stream rings. A quasigeostrophic model is set with a horizontal resolution of 9 km and 6 vertical levels to resolve the mean stratification of the Gulf Stream region.

The results show that the baroclinic merging is slower than the purely barotropic process. The merging is shown to occur in two phases: the first, which produces clove-shaped vortices and diffusive mixing of vorticity contours; and the second, which consists of the sliding of the remaining vorticity cores with a second diffusive mixing of the internal vorticity field. Comparison among Nof, Cushman–Roisin, Polvani et al., and Dewar and Killworth merging events indicates a substantial agreement in the kinematics of the process.

Parameter sensitivity experiments show that the decrease of the baroclinicity parameter of the system, Γ^2, [defined as $\Gamma^2 = (D^2 f_0^2)/(N_0^2 H^2)$], increases the speed of merging while its increase slows down the merging. However, the halting effect of baroclinicity (large Γ^2 or small Rossby radii of deformation) reaches a saturation level where the merging becomes insensitive to larger Γ^2 values. Furthermore, we show that a regime of small Γ^2 exists at which the merged baroclinic vortex is unstable (metastable) and breaks again into two new vortices. Thus, in the baroclinic case the range of Γ^2 determines the stability of the merged vortex.

We analyze these results by local energy and vorticity balances, showing that the horizontal divergence of pressure work term $[\nabla \cdot (p\mathbf{v})]$ and the relative-vorticity advection term $(\mathbf{v} \cdot \nabla \nabla^2 \psi)$ trigger the merging during the first phase. Due to this horizontal redistribution process, a net kinetic to gravitational energy conversion occurs via buoyancy work in the region external to the cores of the vortices. The second phase of merging is dominated by a direct baroclinic conversion of available gravitational energy into kinetic energy, which in turn triggers a horizontal energy redistribution producing the final fusion of the vortex centers. This energy and vorticity analysis supports the hypothesis that merging is an internal mixing process triggered by a horizontal redistribution of kinetic energy.

1. Introduction

Real examples of the merger of two oceanic eddies were obtained both by Cresswell (1982) in the East Australian current system and by Robinson et al. (1986) in the northeast Pacific. Recently there have been numerous numerical and analytical studies about the interactions of isolated vortices, but in spite of the importance of the merger process there is still a limited understanding of the nonlinear dynamics of interacting oceanic vortices.

The merging of two isolated inviscid eddies was considered as a paradox by Gill and Griffiths (1981), who pointed out that in a reduced gravity model, conserving potential vorticity and mass during the process, the final vortex would have energy that is larger than the sum of the individual energies. A series of numerical and laboratory experiments demonstrated that two like-signed vortices merge under a wide set of conditions. Thus, many authors tried to justify the merging process against the Gill and Griffiths paradox by using numerical simulations and laboratory experiments.

The numerical work on the nonlinear processes involved in the interactions of vortices has been done either for purely two-dimensional flows or simplified two-layer density stratification systems. Collision between isolated modons was examined for the quasigeostrophic, barotropic equations by McWilliams and Zabusky (1982). For a range of parameters they observed "inelastic" effects including vorticity filamentation and modon "capture" or "fusion" in an overtaking collision. Overman and Zabusky (1982) studied with contour dynamics algorithms the instability, merger, and breaking of two piecewise-constant finite-area vortex regions. They show that the inviscid merger process may be viewed as the long time evolution of an *instability* of the perturbed vortex regions.

Similar results have been obtained by Melander et al. (1987) who examined the merging of two identical

Corresponding author address: Dr. Nadia Pinardi, IMGA-CNR, via Emilia EST, 770, 41100 Modena, Italy.

regions of uniform vorticity using an approximation to the 2D Euler equations. Using an analytical model, they obtained a necessary and sufficient condition for merger. This merging condition involves only parameters contained in the initial condition and the conserved quantities. Melander et al. (1988) using both an analytical and a numerical model claimed that merging is a process driven by filament formation and caused by the same mechanism as for a single vortex. In fact, Melander et al. (1987) had previously shown that a single-signed sufficiently eccentric vortex relaxes toward axisymmetry by filament generation, which breaks the elliptical symmetry.

Griffiths and Hopfinger (1986) conducted laboratory experiments with geostrophic vortices in a two-layer density stratification. They showed that the combination of two vortices of opposite sign in different layers, called hetons, tear each other apart over a distance of order one Rossby radius or less, while they repel each other if separated by greater distance. They also observed that real vortices of like sign in the same layer coalesce when they approach sufficiently close to each other. This occurred most often when the internal Rossby radius of deformation was large. In another work Griffiths and Hopfinger (1987) suggested that the paradox of merging is resolved by releasing kinetic energy in the eddy exterior. In their experiments, the development of two "spiral arms" of core fluid conserves angular momentum and, through the detrainment of volume from the vortex cores, may also allow merging to continue without an increase of the potential energy.

Nof and Simon (1987) suggested that the potential vorticity of the eddies is altered during their interaction by some mechanism that is not a simple frictional decay and that no external source of energy is needed for the merging. The interaction of two isolated lenslike eddies was examined with the aid of an inviscid nonlinear model by Nof (1988). He argues that the alteration of potential vorticity necessary for the merging to occur is probably achieved via the action of shock waves in the nose of intrusions that develop during the merging process. The final merger vortex is formed by a padlock system of long filaments coming from the original single vortices.

The paradox of merging of Gill and Griffiths was resolved by Cushman-Roisin (1989) noting that the merging of two reduced gravity vortices need not be complete. The final state consists of a center eddy containing almost all the energy but only a fraction of the mass, surrounded by a pair of thin filaments holding the mass difference, a residual of energy, and most of the angular momentum. Thus, filament formation seems to have the crucial role of restoring global energy and mass balances.

Dewar and Killworth (1990) suggested that vortex merger can be energetically permissible even with perfect mass and potential vorticity conservation. If two eddies interact a potential vorticity mixing is started that can have the effect of altering the momentum distribution in the exterior. The disruption of the integrity of the external flow can provide a mechanism for release of potential energy, thus allowing a merger to be possible.

Polvani et al. (1989) used a quasigeostrophic two-layer model to describe the evolution of a merging process in the limit of a small Rossby number. They determined that the merging dynamics of vortices confined in the upper layer is similar to two-dimensional inviscid Euler dynamics. For the equivalent barotropic model (lower layer infinitely deep) they showed that on scales of a few deformation radii, the process of filamentation is greatly suppressed, and thus axisymmetrization almost totally inhibited.

More on the line of our work, Griffiths and Hopfinger (1987) suggested that the density stratification can modify interactions between vortices through the effects of the baroclinic component of the velocity field. They say also that the influence of buoyancy forces is such that it can oppose the increase in potential energy of the flow, which must occur in the absence of sufficient dissipation (Hogg and Stommel 1985). Robinson et al. (1986) gave evidence of the importance of the density stratification on the merging process: they performed a set of sensitivity experiments, showing that increasing the baroclinic effects caused the merger to occur more slowly. Verron et al. (1990) showed that the influence of density stratification on merging depends strongly on the initial shape of the vortices. This is provisionally interpreted as a consequence of the different far-field flow patterns for the different vortex profiles.

All previous numerical and analytical studies have dealt with either two-dimensional systems or at most two-layer systems. In this study we present instead six-level, realistic stratification numerical experiments in order to understand how the baroclinicity can influence the merging of realistic ringlike vortices. The stratification is chosen to be representative of the Gulf Stream free jet regime. We also use realistic horizontal vortex structures as described by Olson (1980) for cyclonic rings. The rings have an "interior" velocity field in near-solid body rotation, surrounded by a front that exhibits a maximum of the velocity field and a discontinuity in the relative vorticity field. This velocity profile is similar to Griffiths and Hopfinger (1987) and it is also vertically sheared. The invariance of the quasigeostrophic vorticity equation for $\{\psi, y\} \leftrightarrow \{-\psi, -y\}$ transformations allows us to deduce the merging dynamics of anticyclonic rings from the simulations of cyclonic rings. Thus, throughout the paper, we will use only cyclonic rings.

In section 2 we describe the model parameters and the numerical experiments. In section 3 we compare the baroclinic merging process with the barotropic case, and in section 4 all the baroclinic sensitivity experiments are analyzed in detail. Finally, in section 5 we

show the results of the energy and vorticity analysis in order to interpret the dynamics of the merging events.

2. Model setup and numerical experiments

The model used for these numerical simulations is the Harvard Open Ocean Model (Robinson and Walstad 1987). It is a regional quasigeostrophic dynamical model that has been developed for realistic local dynamical studies of fundamental processes and real data initialization.

The nondimensional potential vorticity equation is written:

$$\frac{\partial q}{\partial t} + \alpha J(\psi, q) + \beta \frac{\partial \psi}{\partial x} = F_{ijk}, \tag{1}$$

where

$$q = \nabla_H^2 \psi + \Gamma^2 \frac{\partial}{\partial z}\left(\sigma \frac{\partial \psi}{\partial z}\right) \tag{2}$$

and the Jacobian is defined as

$$J(\psi, q) = \frac{\partial \psi}{\partial x}\frac{\partial q}{\partial y} - \frac{\partial \psi}{\partial y}\frac{\partial q}{\partial x}.$$

Here the reader is reminded that we have divided the total pressure and density fields into

$$p = \bar{p}(z) + p'(x, y, z, t)$$
$$\rho = \rho_0 + \bar{\rho}(z) + \rho'(x, y, z, t),$$

and the Rossby number expansion is done on the ρ' and p' fields. For the details of the derivation see Robinson and Walstad (1987). The nondimensional parameters are

$$\alpha = \frac{V_0 t_0}{D}, \quad \beta = \beta_0 D t_0, \quad \Gamma^2 = \frac{f_0^2 D^2}{N_0^2 H^2},$$

where V_0 is a typical fluid velocity, D the horizontal scale of motion, H the vertical scale, f_0 is the constant part of the Coriolis parameter in the region, β_0 is the meridional gradient of the Coriolis parameter defined as

$$\beta_0 = \left.\frac{\partial f}{\partial y}\right|_{y=y_0} = \frac{2\Omega}{a}\cos\theta_0$$

where a is the radius of the earth, Ω is the earth's rotation rate, and θ_0 the central latitude of the domain. The stratification is contained in σ, which is defined as

$$\sigma(z) = \frac{N_0^2}{N^2(z)},$$

where

$$N^2 = -\frac{g}{\rho_0}\frac{\partial \bar{\rho}}{\partial z},$$

and N_0 is a typical main thermocline Brunt–Väisälä frequency.

The horizontal part of the potential vorticity q, $R = \nabla_H^2 \psi$, is called *relative vorticity,* the vertical part $T = \Gamma^2(\partial/\partial z)[\sigma(\partial\psi/\partial z)]$ is called *thermal vorticity,* while $\beta_0 y$ is the planetary vorticity. We symbolically rewrite (2) as

$$Q = R + T.$$

Hereafter Γ^2, called the baroclinicity parameter, can also be defined as $\Gamma^2 = d^2/R_0^2$, where $R_0^2 = N_0^2 H^2/f_0^2$ is approximately the first Rossby radius of deformation for our stratification (Robinson et al. 1988). The Γ^2 values differentiate between the barotropic regime ($d^2 \ll R_0^2$ and small Γ^2) and the baroclinic regime ($d^2 \gg R_0^2$ and large Γ^2). In other words, Γ^2 is the ratio between relative and thermal vorticity components that can be increased (decreased) by increasing (decreasing) d with respect to R_0. A large R_0 with respect to d means that there is no strong baroclinic coupling between the levels and that the barotropic mode of the stratified system has the highest amplitude (Rhines 1977).

The rhs of Eq. (1), F_{ijk}, is the schematic representation of the Shapiro filter of order i, applied j times and every k time steps to q (Shapiro 1970, 1971). We choose $p = 4$, $q = 1$, and $r = 1$. This corresponds to an eight-order Laplacian operator plus mixed derivatives as shown in Shapiro (1971). This filter removes small-scale vorticity, which cascades from larger to smaller scales in nonlinear flows via two-dimensional or geostrophic turbulence processes (Rhines 1979; and Robinson and Walstad 1987).

The computational model has been calibrated by Haidvogel et al. (1980) and Miller et al. (1983). The open horizontal boundary conditions are those specified by Charney et al. (1950), that is, the streamfunction specified everywhere on the boundary and vorticity specified at inflow points. The mathematical problem

TABLE 1. Model symbols, parameters, and scale factors. [Adapted from Robinson et al. (1988)].

Symbol	Definition
V_0	velocity scale: 40 cm s^{-1}
t_0	time scale: 4 days
D	horizontal scale: 40 km
f_0	Coriolis parameter at $\theta_0 = 39°$N (9.1×10^{-5} sec^{-1})
β_0	$\partial f/\partial y\|_{\theta=\theta_0} = 1.8 \times 10^{-11}$ (m s^{-1})$^{-1}$
N_0^2	midthermocline Brunt–Väisälä frequency value
H	vertical scale: 700 m
$N^2(z)$	climatological Brunt–Väisälä profile
ϵ	$(f_0 t_0)^{-1} = 0.03$ Rossby number
α	$t_0 V_0/D = 3.456$
β	$\beta_0 t_0 D = 0.2558$
Γ^2	$f_0^2 D^2/(N_0^2 H^2) = 1.411$
$\sigma(z)$	$N_0^2/N^2(z)$: stability profile
ψ	geostrophic streamfunction or pressure
F_{pqr}	Shapiro filter (p: order, q: frequency, r: which time step)

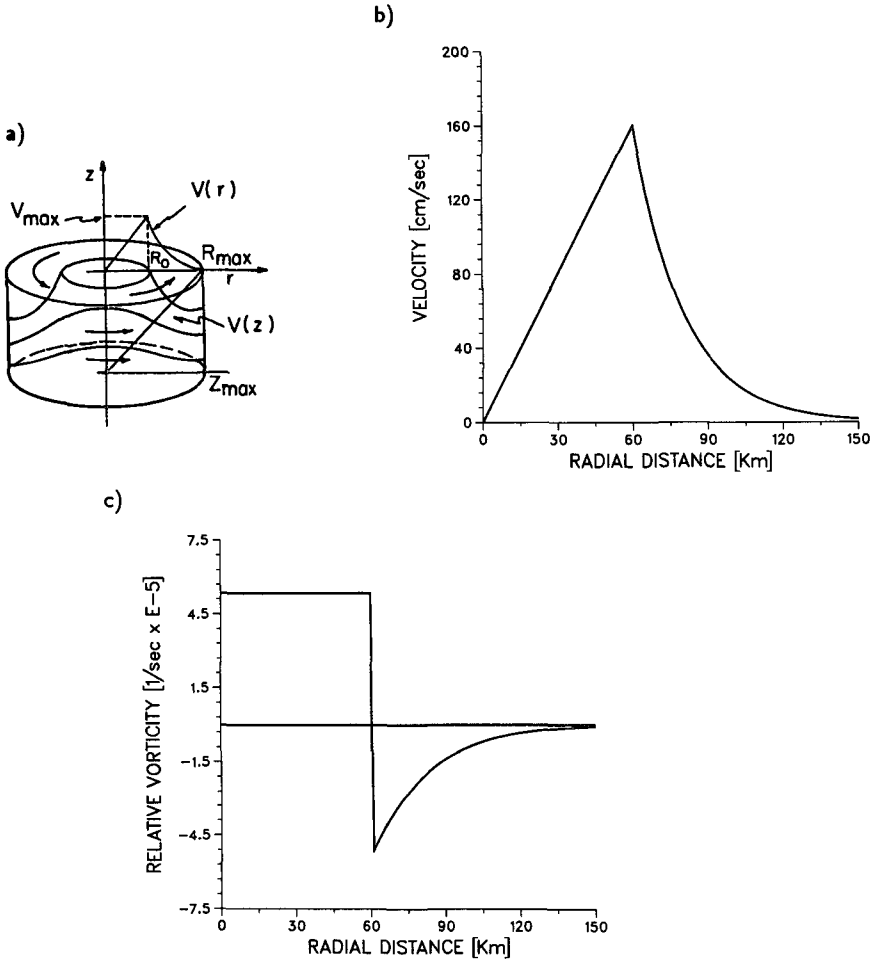

FIG. 1. (a) Schematic of a baroclinic ringlike vortex structure developed by Robinson et al. (1988). (b) Tangential velocity structure of the initial vortex. (c) Relative vorticity as a function of radial distance.

will be closed by the specification of an initial condition for ψ and q.

For the present purpose of modeling vortices, the side boundaries are specified as closed; for example, the streamfunction is imposed to be constant along the walls together with the initial vorticity. However, we do not conserve mass in the domain since we do not impose the integral constraint

$$\int\int \frac{\partial w}{\partial z}\, dxdy = 0$$

(Pinardi and Milliff 1989). Our model results are not affected by the presence of the boundaries for the length of the integrations presented.

To find the numerical values of the model parameters α and β, we used the nondimensional time, space, and velocity values listed in Table 1. The scales of motion were chosen to reflect the dynamics of the Gulf Stream system as discussed in Robinson et al. (1988). The horizontal resolution is 9 km, the total domain is 131×81 grid points (1170×720 km^2), and the time step is one-half hour. We use six levels in the vertical located at 100, 300, 700, 1100, 2150, and 3625 m as in Robinson et al. (1988).

The initial condition is represented by two equal cold (cyclonic) baroclinic vortices whose initial separation distance d is measured from their centers surrounded by still water. In order to calculate the appropriate streamfunction and vorticity fields for model initialization, an analytic expression for the velocity structure of the two vortices is assumed. We use the "feature model" for Gulf Stream rings that has been used in ocean forecast experiments (Robinson et al. 1988). The tangential velocity increases linearly from zero at the center out to a maximum $V_{\max}$ at a radius r_0:

$$v(r) = \frac{V_{\max}}{r_0} r \quad \text{for} \quad r < r_0, \tag{3}$$

while outside r_0 the velocity decays exponentially:

$$v(r) = V_{\max} e^{a[1-(r/r_0)]} \quad \text{for} \quad r > r_0. \tag{4}$$

The parameters of the vortex feature model are thus given by the maximum velocity $V_{\max}$, the radius of maximum velocity r_0, and the exponential decay factor a. The velocity decreases linearly in the vertical [$v(z)$ in Fig. 1a] and becomes zero at a depth $z_{\max}$ in order to represent a real vortex that has a nonzero velocity field only above the thermocline. A schematic of the vortex model and its associated parameters is shown in Fig. 1a. The standard parameters for the vortices employed by McGillicuddy (1987) and Robinson et al. (1988) are

$$V_{\max} = 160 \text{ cm s}^{-1}, \quad r_0 = 60 \text{ km}, \quad a = 3, \quad z_{\max} = 1000 \text{ m}.$$

From the expressions (3) and (4) we can write the geostrophic streamfunction and vorticity fields for the model initialization. The analytic streamfunction is written as

$$\psi(r) = \int \frac{V_{\max}}{r_0} r dr = \frac{V_{\max}}{2r_0} r^2 + c_1 \quad \text{for} \quad r < r_0 \tag{5}$$

$$\psi(r) = \int V_{\max} e^{a[1-(r/r_0)]} dr = -V_{\max} \frac{r_0}{a} e^{a[1-(r/r_0)]} + c_2 \quad \text{for} \quad r > r_0. \tag{6}$$

Assuming continuity in the streamfunction field, we obtain

$$c_2 = \frac{V_{\max}}{2r_0} r_0^2 + \frac{V_{\max}}{a} r_0,$$

and can choose $c_1 = 0$. We obtain the relative vorticity field, R, calculating the Laplacian of the streamfunction in polar coordinates, which results in

$$R = \begin{cases} 2\dfrac{V_{\max}}{r_0}, & r < r_0 \quad (7) \\ V_{\max} e^{a[1-(r/r_0)]}\left(-\dfrac{a}{r_0} + \dfrac{1}{r}\right), & r > r_0. \quad (8) \end{cases}$$

In Figs. 1b and 1c analytical velocity and relative vorticity profiles are shown. This velocity profile is also produced by Griffiths and Hopfinger (1987) in their laboratory experiments, and for $r < r_0$ is the same of Rankine vortices. Equations (5), (6), (7), (8) give the ψ and R fields of one vortex. The model initial condition uses the superposition of two of these analytical expressions to construct a field containing two nearby vortices. To get q for the model initialization the thermal vorticity is calculated from the ψ field and the baroclinic modes. The flow field for $r > r_0$ will be indicated as an external flow field to compare our energy analysis with previous results. The core of the vortices is indicated by the region $r < r_0$, for example, the region of positive and constant values of R.

TABLE 2. Run table. The nondimensional model parameter symbols are explained in Table 1; $V_{\max}$ represents the maximum vortex speed measured in cm s^{-1}, d the vortices separation in km/multiple of r_0 and $z_{\max}$, the maximum depth of the vortex in meters.

	Initial condition parameters			Nondimensional model parameters		
Run	d	$V_{\max}$	$z_{\max}$	α	β	Γ^2
BT1	144/2.4	160		3.456	0.2558	0
BC1	144/2.4	160	1000	3.456	0.2588	1.411
BC2	144/2.4	100	1000	3.456	0.2558	1.411
BC3	126/2.1	160	1000	3.456	0.2558	1.411
BC4	162/2.7	160	1000	3.456	0.2558	1.411
BC5	144/2.4	160	500	3.456	0.2558	1.411
BC6	144/2.4	160	2000	3.456	0.2558	1.411
BC7	144/2.4	160	1000	1.0	0.2558	1.411
BC8	144/2.4	160	1000	3.456	0	1.411
BG1	144/2.4	160	1000	3.456	0.2558	0.1
BG2	144/2.4	160	1000	3.456	0.2558	0.2
BG3	144/2.4	160	1000	3.456	0.2558	0.3
BG4	144/2.4	160	1000	3.456	0.2558	0.4
BG5	144/2.4	160	1000	3.456	0.2558	0.5
BG6	144/2.4	160	1000	3.456	0.2558	0.6
BG7	144/2.4	160	1000	3.456	0.2558	0.7
BG8	144/2.4	160	1000	3.456	0.2558	0.8
BG9	144/2.4	160	1000	3.456	0.2558	0.9
BG10	144/2.4	160	1000	3.456	0.2558	2.8
G2	144/2.4	160	1000	3.456	0.	0.2
G3	144/2.4	160	1000	3.456	0.	0.3
G4	144/2.4	160	1000	3.456	0.	0.4
G5	144/2.4	160	1000	3.456	0.	0.5
G6	144/2.4	160	1000	3.456	0.	0.6
G7	144/2.4	160	1000	3.456	0.	0.7

To understand the merging dynamics of axisymmetric baroclinic vortices we performed a set of sensitivity experiments, changing both the initial condition parameters and the nondimensional model parameters; these are listed in Table 2.

3. Barotropic–baroclinic merger comparison

In this section, we analyze the differences between the BT1 (barotropic) and BC1 (standard baroclinic) experiments, shown in Fig. 2. In all of the baroclinic figures we will show only the vorticity fields at the first level of the model, that is, at the depth $z = 100$ m. This is the level at which the barotropic and baroclinic initial ψ profiles are identical. This is also the level at which the fastest merging in the baroclinic case is achieved.

In the barotropic case the merging process starts on the second day. This means that positive contour lines belonging to the vorticity cores of the single vortices are beginning to encircle both vortices. On the third day the barotropic case shows the merging process well under way, and on day 5 the two vortices are completely merged. In the baroclinic case the process is still evolving on days 3 and 5, and it will be completed only after 11 days. The slow merging in the baroclinic case

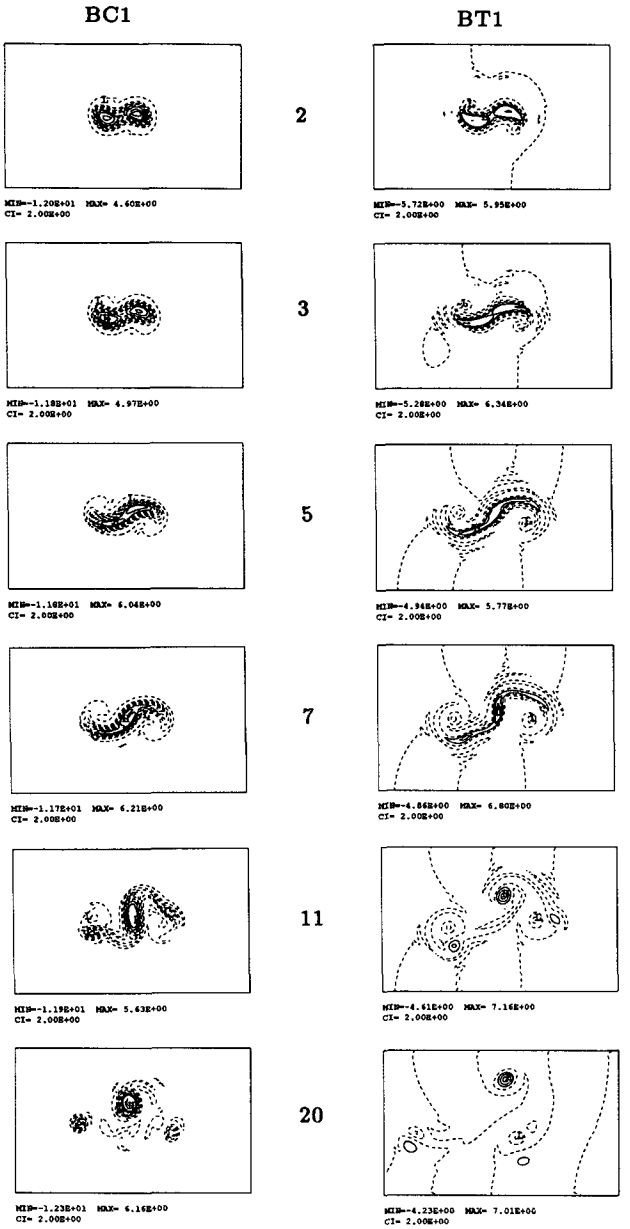

FIG. 2. Comparison between BT1 and BC1 experiments: relative vorticity field. The two different experiments are indicated at the top. Time in days is displayed at the center. The maximum, minimum, and contour interval are displayed below each picture. Dashed contours correspond to negative values and continuous lines to positive values. The first dashed closed contour after a continuous line represents the zero-contour level.

means that the presence of the baroclinicity parameter (Γ^2) in (1) inhibits the dynamical evolution of the merging process.

Comparing the two experiments of Fig. 2 it is clear that the baroclinic merging case is not only slower but qualitatively different from the barotropic case. We see that after only two days the interacting vortices form a characteristic "S"-shaped area that contains the combination of the two merging vortices and the developing arms at the opposite extremities of the interacting region. The arms are due to a process of vorticity filamentation, which is the result of a two-dimensional turbulent cascade (Melander et al. 1987). The S-shaped area rotates anticlockwise faster in the barotropic than baroclinic case. The faster the merging, the faster the rotation rate. We can also see at the same time the presence of two small vortices called "near field" vortices in the upper left and lower right of the S. They are located near the forming arms and have vorticity cores of opposite sign with respect to the initial merging vortex cores. It is clear from Fig. 2 that the near-field vortices do not develop in the baroclinic case. In the barotropic case, they probably form as a mechanism to equilibrate locally the increase in curvature of the vorticity field. A horizontal vorticity redistribution process is triggered to balance the local increase of vorticity accumulating in the arms, and it produces the closed circulation of the near-field vortices. If vortex stretching (baroclinicity) is present, the near-field vortices do not need to be generated because relative vorticity can be transformed into thermal vorticity without triggering the local horizontal redistribution process. In the energy analysis section below we find that in the region of the near-field vortices a net conversion of kinetic to available gravitational energy occurs, thus supporting the interpretation that relative vorticity (kinetic energy) could change into stretching or vertical shear vorticity (available gravitational energy). Furthermore, it is clear that the barotropic near-field vortex formation process is not essential to the merging event because it also appears in the case in which the vortices

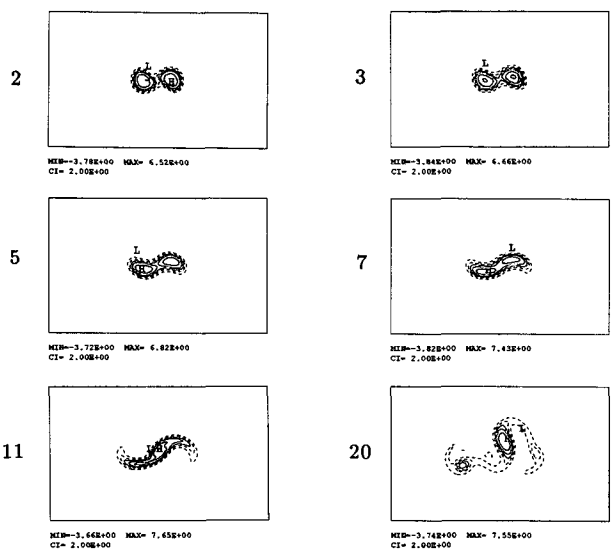

FIG. 3. Relative vorticity field for the BC2 experiment. Time in days is indicated on the left. The contour conventions are described in the caption of Fig. 2.

do not merge at all, as shown by Masina and Pinardi (1991) for the purely barotropic case.

In the barotropic case the developed long and thin arms accumulate vorticity at their ends. Eventually the vorticity forms patches corresponding to closed contours. These new patches at the extremities of the arms are called secondary vortices [also called satellite vortices in Pavia and Cushman-Roisin (1990)]. They can detach from the merger vortex forming two dipolar structures with the two near-field vortices. In the baroclinic case the vorticity filamentation that characterizes the two-dimensional enstrophy cascade to small scales

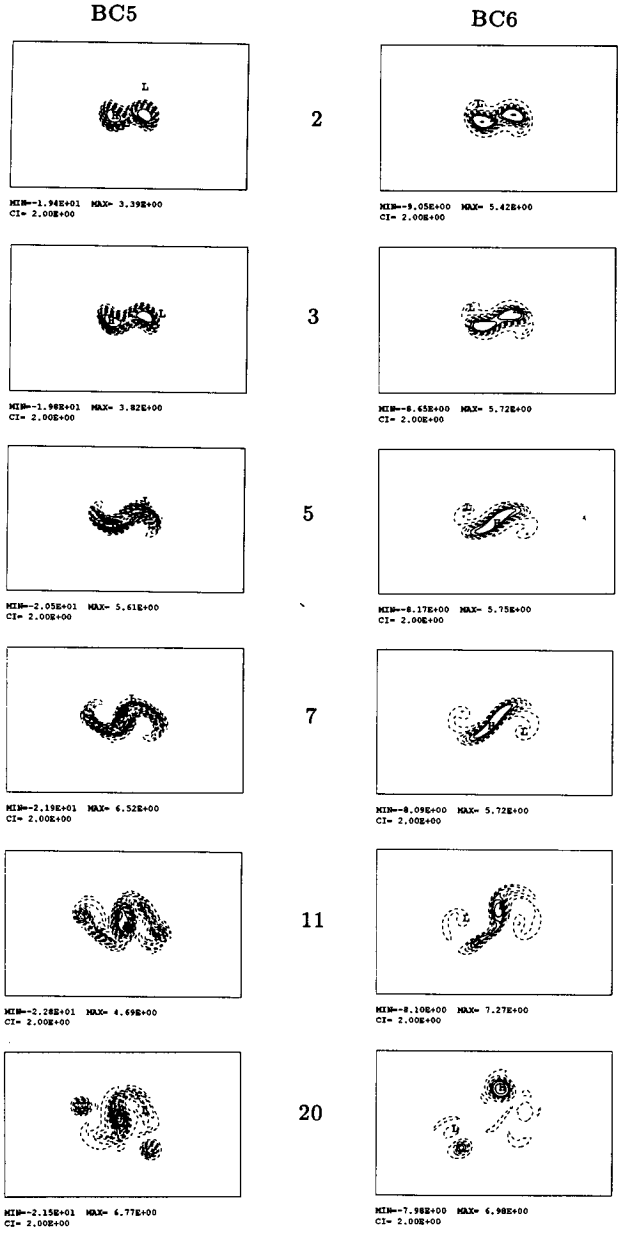

FIG. 4. As in Fig. 2 but for the BC5 and BC6 cases.

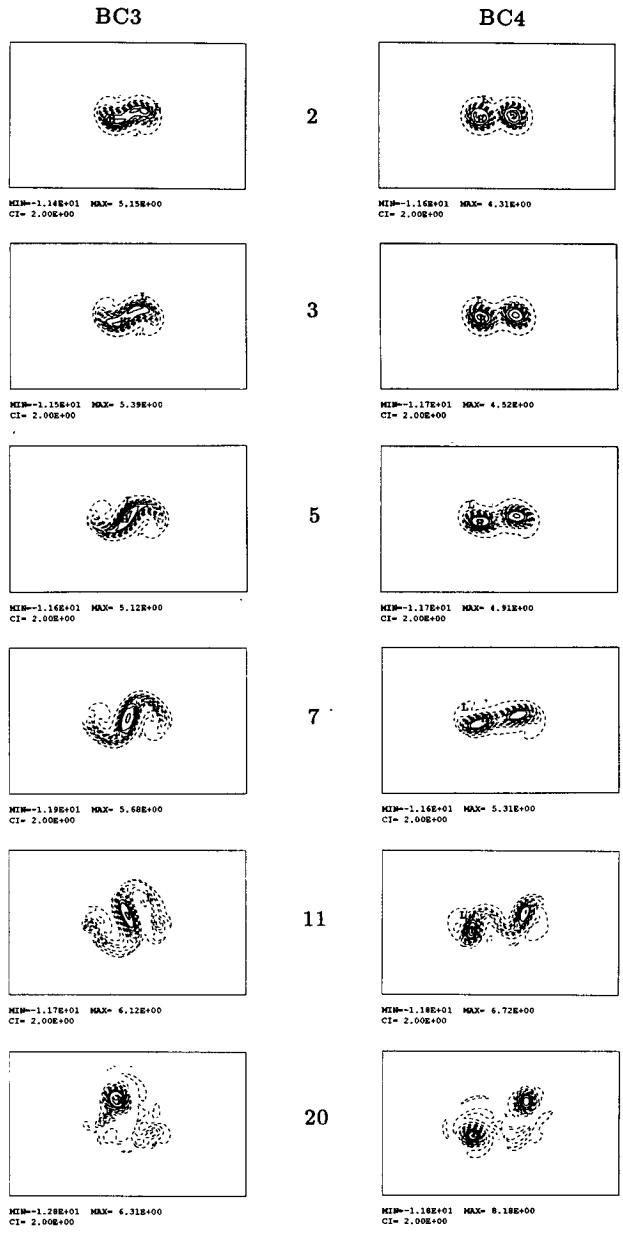

FIG. 5. As in Fig. 2 but for the BC3 and BC4 cases.

is clearly inhibited. Thus, a slower merging process produces thicker arms and stronger secondary vortices that detach from the merger structure later than in the purely barotropic case. In the baroclinic case the secondary vortices are monopoles since there are only very weak near-field vortices.

4. Baroclinic vortex-merger sensitivity experiments

a. Initial condition parameter variations

In Fig. 3 we show the BC2 experiment, obtained by decreasing the value of the initial maximum vortex

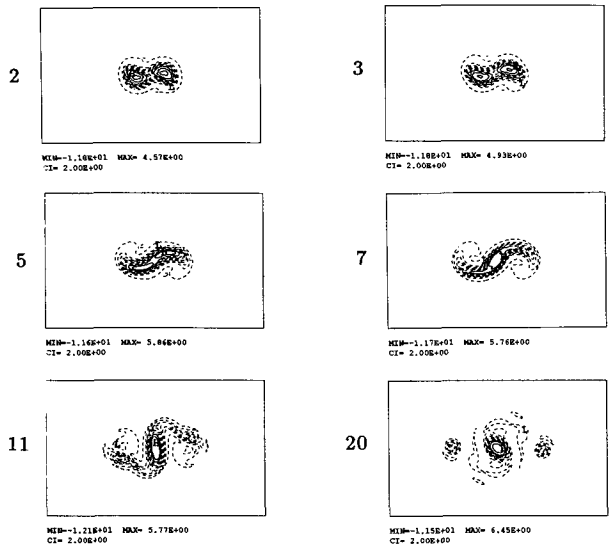

FIG. 6. As in Fig. 3 but for the BC8 case.

speed to 100 cm s^{-1}. In this case the merging rate is slowed down, as seen by comparing day 7 in Figs. 2 and 3. The dynamical behavior of BC1 and BC2 is the same, but in the BC2 case the processes such as the "S"-shaped formation and the counterclockwise rotation of the merger structure are slower. Even after 20 days the BC2 case does not complete the detachment of the secondary vortices from the merger structure. We can then conclude that the initial horizontal shear structure of the rings determines the merging rate and the development of the arms. This case, as the barotropic one discussed before, brings evidence toward the conclusion that the merging is triggered by a process of horizontal redistribution of vorticity that is clearly very sensitive to the initial horizontal shear of the velocity field.

In Fig. 4 we compare the BC5 and BC6 runs. In these two experiments we changed only the maximum depth of the vortex (500 m and 2000 m instead of the standard value, 1000 m). Already after 3 days it is clear that shallow vortices (left column) merge slower than deep ones (right column). The behavior of the slower case is similar to the standard one, even if the BC5 case produces stronger arms and consequently stronger secondary vortices. The BC5 merger structure is still showing vorticity filamentations after 20 days meaning that the process of axisymmetrization of the merger vortex is still occurring. The BC6 run shows the development of near-field vortices as in the barotropic case even if they are weaker. The deeper vortices, thus, behave in a manner similar to the purely barotropic case.

The comparison between the BC3 and the BC4 runs is presented in Fig. 5, where the initial separation distance between the two vortices is changed. The left column shows the evolution of two vortices separated initially by a distance $d = 2.1r_0$, while in the right column $d = 2.7r_0$, where r_0 is the vortex radius. The vortices of the BC4 experiment do not merge; thus, our critical initial separation distance is $d = 2.4r_0 \pm 2\Delta x = (2.4 \pm 0.3)r_0$. Melander et al. (1987) obtained a critical distance $d = 3.4r_0$, which was confirmed by a value of $(3.3 \pm 0.2)r_0$ found by Griffiths and Hopfinger (1987). Comparing BC1 with BC3 it is clear that a smaller initial separation distance of the vortices increases the merging rate. In the case of no merging we can follow for each vortex the characteristic evolution of a single vortex: the counterclockwise rotation and

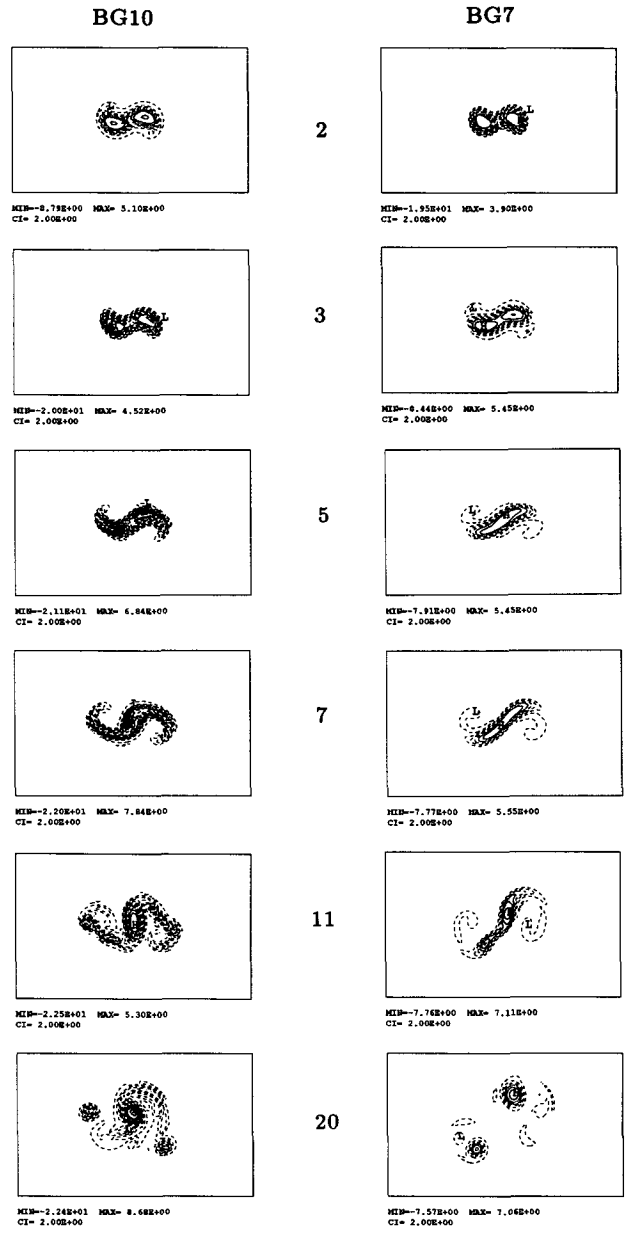

FIG. 7. As in Fig. 2 but for BG7 and BG10 cases.

the process of vorticity filamentation that is particularly active in the area between the two vortices.

In conclusion, the initial condition sensitivity experiments show that higher values of relative vorticity and kinetic energy in the initial condition produce faster merging processes. Slow (small V_{max}) and shallow vortices merge slower than fast and deep ones. The abundance of vorticity filamentation in the arms is also controlled by the speed of merging. Near-field vortices are produced by deep initial vortices, which merge rapidly as in the barotropic case.

b. Environmental parameter variations

In this section we will show experiments obtained by changing the nondimensional parameters of Eq. (1).

In Fig. 6 the BC8 run with $\beta = 0$ is presented. Comparing Fig. 2 for the BC1 case and Fig. 6, it is evident that the merging rate is not affected by the value of the β parameter. The difference between BC1 and BC8 is evident in the formation of the arms. In the BC8 case the arms are completely symmetric, and the final state is composed by three monopoles that do not show any westward shift.

In Fig. 7 we compare BG7 ($\Gamma^2 = 0.7$, right column) and BG10 ($\Gamma^2 = 2.8$, left column) experiments. Comparing these two experiments with the BC1 standard case of Fig. 2, it is evident that the decrease of the baroclinicity parameter of the system increases the speed of merging. In fact, after 5 days the vortices with the smallest baroclinicity parameter are completely merged; the ones with the standard baroclinicity parameter are still merging, while the ones with the largest baroclinicity parameter are too far to merge. However, after day 5 the $\Gamma^2 = 2.8$ starts to evolve in a similar way to the BC1 case, and at day 20 BG10 and BC1 are similar, while they are both very different from BG7. Thus, decreasing the Γ^2 parameter has a greater impact on the merging process than the increase of Γ^2. For large Γ^2 we reach a saturation limit, and the merging process, after an initial slowdown, occurs as for smaller Γ^2 values. These results are in agreement with Griffiths and Hopfinger (1986) results, which showed that merging will be favored by larger initial Rossby radii of deformation (small Γ^2).

The comparison of these experiments with the ones obtained by changing the maximum depths of the initial vortices shows marked analogies. The dynamical evolution of the runs of Fig. 7 are so similar to those of Fig. 4 that we can deduce that the depth of the initial vortices and the baroclinicity parameter affect the merging process in a similar way. In particular, deep vortices correspond to shallower vortices embedded in a smaller Γ^2 environment and vice versa.

In Fig. 8, BG1 ($\Gamma^2 = 0.1$) and BG4 ($\Gamma^2 = 0.4$) runs are shown. The simulation with the smallest baroclinicity parameter is the fastest among the baroclinic runs (its merging speed is more or less equal to the barotropic case). Like the barotropic case, it clearly shows the presence of two near-field vortices at the extremities of the arms. The arms do not develop as strongly as in the barotropic case due to a still-weaker vorticity filamentation process with respect to the purely barotropic case.

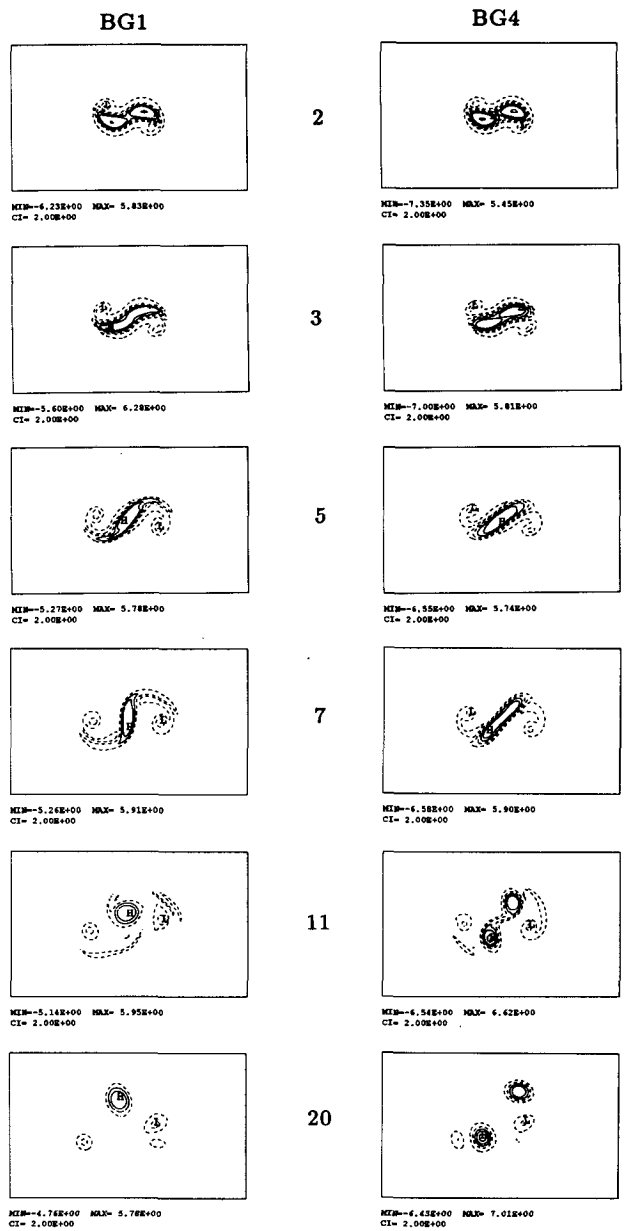

FIG. 8. As in Fig. 2 but for BG1 and BG4 cases.

The simulation with $\Gamma^2 = 0.4$ shows a new dynamical process. In this case the merger structure developed through the merging process is not stable. In fact, even if the initial vortex cores seem to be completely merged at day 5, they actually are only sliding one on the other (see section 5). After day 7 they will split up, forming

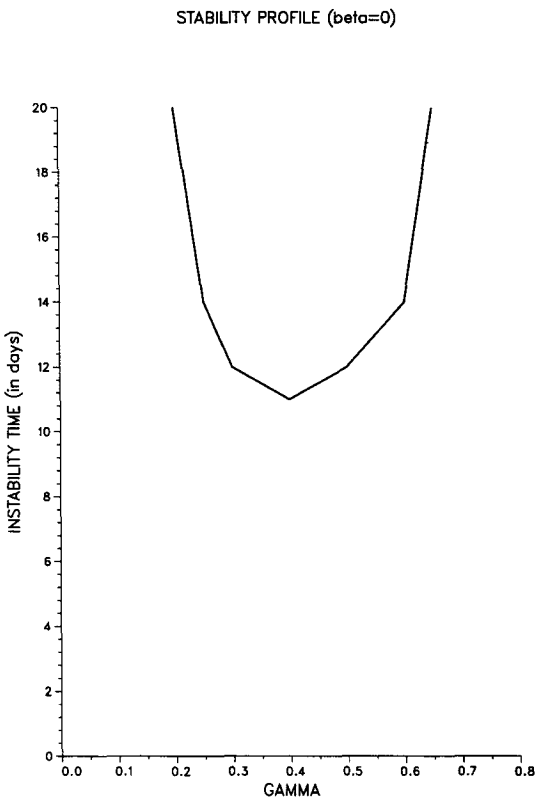

FIG. 9. Stability profile: on the x axis Γ^2 values, on the y axis the time t_I in days before the splitting of the merger vortex with the assumption of $t_I = \infty$ for the stable vortex.

two separate structures again. Scanning all possible values of Γ^2 by an interval of 0.1, we found that a range of critical values of the baroclinicity parameter exists, for which the merging produces a metastable merger vortex with a life of several days, which subsequently splits into two new vortices. Figure 8 shows an example of such metastable merger vortex for $\Gamma^2 = 0.4$. Indicating with t_I the time before the splitting of the merger vortex (11 days for BG4, ∞ for a stable

TABLE 3. Energy equation symbols.

Symbol	Physical process	Dimensional form
K	Kinetic-energy density	$(u^2 + v^2)/2$
A	Available gravitational energy density	$g\rho'^2/2s$
$\dot{K}$	Time rate of change of K	$\partial K/\partial t$
ΔF_k	Horizontal kinetic energy *advective* working rate	$-[\partial(uK)/\partial x + \partial(vK)/\partial y]$
δf_k	Vertical kinetic energy *advective* working rate	$-\partial(wK)/\partial z$
ΔF_π	Horizontal *pressure* working rate	$-[\partial(pu)/\partial x + \partial(pv)/\partial y]$
δf_π	Vertical *pressure* working rate	$-\partial(pw)/\partial z$
b	Buoyancy work or interaction working rate	$-\rho' gw$
$\dot{A}$	Time rate of change of A	$\partial A/\partial t$
ΔF_A	Horizontal AGE *advective* working rate	$-[\partial(uA)/\partial x + \partial(vA)/\partial y]$

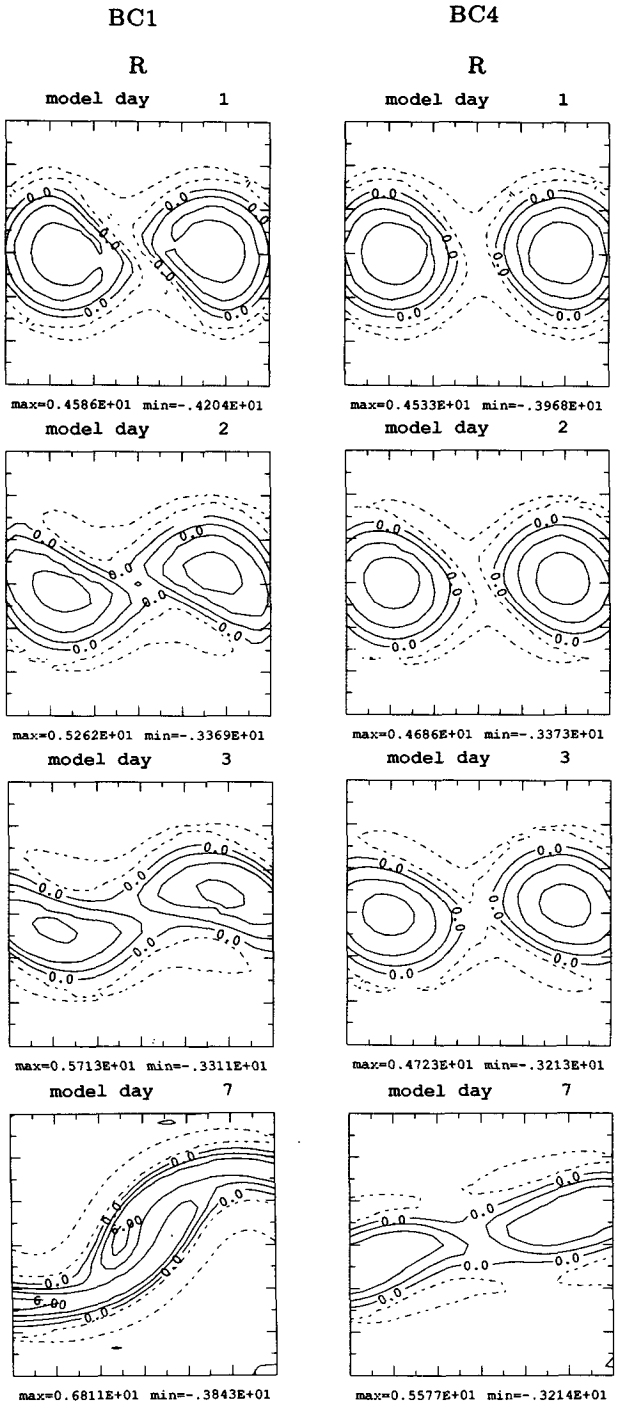

FIG. 10. Relative vorticity fields for BC1 and BC4 experiments at level $z = 300$ m. The two different experiments are indicated at the top. Time in days is displayed at the top of each picture. The maximum and the minimum of the field are displayed below each picture and the contour interval is two nondimensional units.

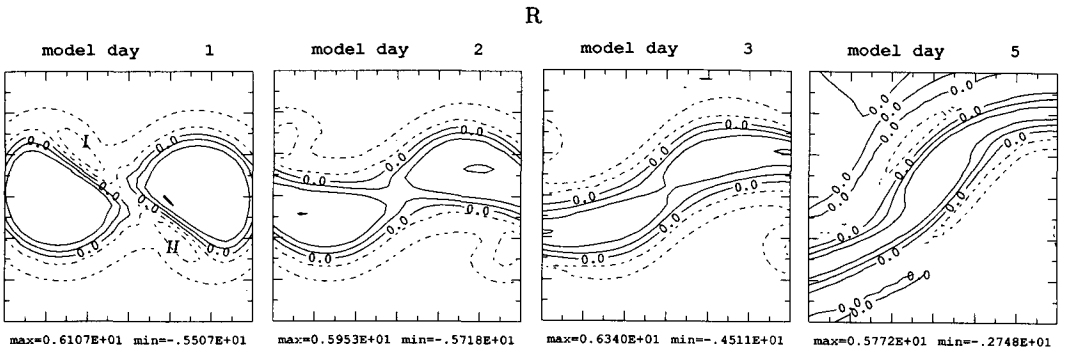

FIG. 11. Relative vorticity field for the BT1 experiment. Time in days is displayed at the top of each picture. The maximum and the minimum are displayed below each picture, and the contour interval is two nondimensional units.

vortex as in the BG1 case), we show in Fig. 9 that t_I is finite for $0.2 < \Gamma^2 < 0.7$. This also means that the lifetime of a merger vortex is finite for a wide range of Γ^2 parameters. In Fig. 9 we used the $\beta = 0$ experiments so that there would be no asymmetric behavior in the development of the arms and less uncertainty in the classification of metastable merging and cutoff of secondary vortices from the arms.

5. Energy and vorticity-analysis results

We now analyze the model results via energy and vorticity analysis (EVA; Pinardi and Robinson 1986, hereafter called PR) to assess the energy conversion and redistribution processes occurring during the merging event. We review some of the formalism and refer to PR for detailed explanation of the derivation of the equations. The kinetic energy, K, equation is written:

$$\frac{\partial}{\partial t} K = -\alpha \nabla \cdot (\mathbf{v}_0 K) - \nabla \cdot (p_1 \mathbf{v}_0 + \mathbf{v}_1 p_0) - \partial_z (p_0 w_1) + \delta_0 w_1 + D \quad (9)$$

$$\dot{K} = \Delta F_K + \Delta F_\pi + \delta f_\pi - b + D, \quad (10)$$

where the "0" and "1" subscripts indicate the zero- and first-order fields in the Rossby number expansion of the equations, $K = (v_0^2 + u_0^2)/2$, $p_0 = \psi$ is the geostrophic pressure or streamfunction; $(u_0, v_0) = (-\psi_y, \psi_x)$, $\dot{K}$ is the time rate of change of K, ΔF_K indicates the divergence of kinetic energy advective fluxes, ΔF_π the horizontal divergence of pressure work energy fluxes, δf_π the vertical divergence of pressure work energy fluxes, and b is the buoyancy work or conversion term between kinetic and available gravitational energy (A). The evolution equation for A is

$$\frac{\partial}{\partial t} A = -\alpha \nabla \cdot (\mathbf{v}_0 A) - \delta_0 w_1 + D \quad (11)$$

$$\dot{A} = \Delta F_A + b + D, \quad (12)$$

where $\dot{A}$ is the time rate of change of A, ΔF_A is the horizontal divergence of advective A fluxes, and b the conversion term. In (10) and (12) D is the dissipation equivalent term in the energy equations due to the filter, F_{pqr}, in the vorticity equation (1). All the symbols are written and explained again in Table 3. For reference we rewrite the vorticity equation as

$$\partial_t(\nabla^2\psi) + \Gamma^2 \partial_t(\sigma\psi_z)_z = -\alpha \mathbf{v} \cdot \nabla(\nabla^2\psi) - \alpha\Gamma^2 \mathbf{v} \cdot \nabla(\sigma\psi_z)_z - \beta\psi_x + F \quad (13)$$

$$\dot{R} + \dot{T} = \Delta F_R + \Delta F_T + \Delta F_P + F, \quad (14)$$

where $\dot{R}$ is the time rate of change of the relative vorticity, $\dot{T}$ the time rate of change of thermal vorticity, ΔF_P the β term, ΔF_R the advection of R, ΔF_T the advection of T, and F the filter.

a. *Vorticity analysis*

We first analyze Q and the vorticity balance fields by showing maps of the various terms in Eqs. (13) and (14). First, we look to the comparison between merging and no merging events in the R fields. We show only the R fields because they are qualitatively similar to the T fields with the addition of smaller-scale components that are shown to be important during the merging. The EVA results are presented hereafter in a smaller domain centered around the interacting vortices.

In Fig. 10, we show such fields at different times of evolution of the merging and no-merging processes. We distinguish two phases in the merging process: the first between day 0 and 4 and the second starting at day 5. During the first phase the merging process is associated with a flattening of the interacting sides of the vortices. The R fields of the merging vortices become shaped like cloves (a clove here represents half of an ellipse), and jets form along the flat sides of the cloves. In the no-merging case these jets do not form as quickly and as strongly as in the merging case. At a second stage of the first phase (day 3 in Fig. 10) the zero contour lines start to fuse via the filtering, acting as a diffusion in the model. This means that the "in-

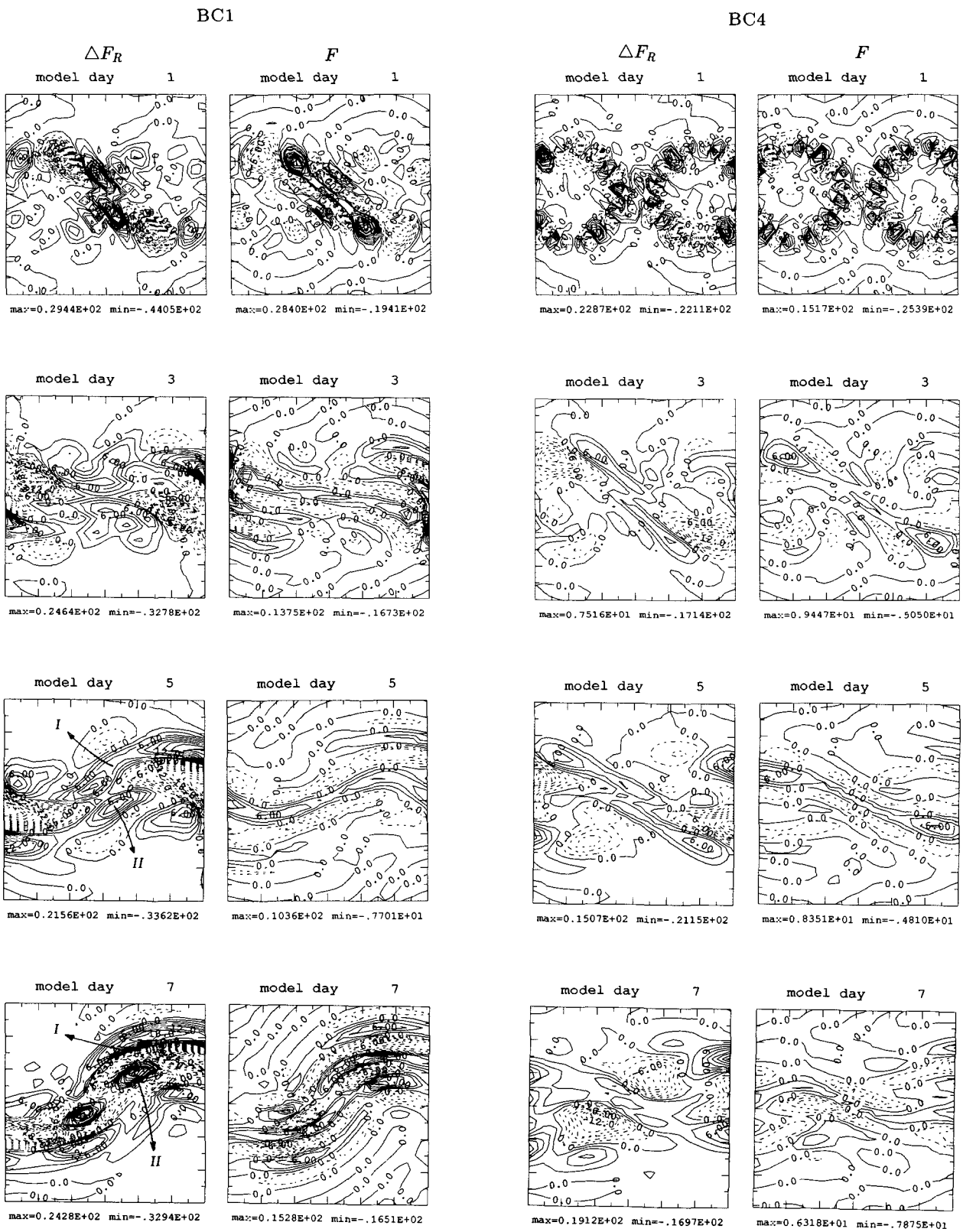

FIG. 12. As in Fig. 10 but for the advection of relative vorticity and the Shapiro filter terms in Eq. (13).

terior" vorticity fields belonging to the cores of the single vortices start to fuse. This process of fusion starts at the nearest points of the cloves.

The second phase of merging consists of the sliding of the remaining vorticity cores toward the center of the future merger structure. In Fig. 10 we show day 7 when the still-separated vorticity cores have formed into intrusions that are sliding until they overlay. At day 11 (not shown) another dissipative merging of contours occurs forming the core of the merger vortex. The no-merging case seems never to reach the vorticity configuration necessary to develop the merging phases as described above.

It is interesting to notice that the same two phases happen in the fully barotropic case as shown in Fig. 11. In addition, for the barotropic case, there is the formation of two patches of negative vorticity (regions I and II in Fig. 11) along the sides of the clove-shaped vortices. These vorticity patches come from the initial central area of interaction of the vortices, and they go to form the anticyclonic near-field vortices of Fig. 2. This initial vorticity expulsion and concentration is inhibited in the baroclinic case as evident by comparing Figs. 10 and 11.

It is interesting to notice that the results of Polvani et al. (1989) obtained with contour dynamics algorithms, show qualitatively the same two-phase process of vortex merging. Their initial vortices shape up as cloves and slide one above the other as in our case. Naturally the diffusive merging in their case does not occur. The phenomenology seems, however, similar.

It is important to note that our description of the vorticity processes points to changes in the "internal" (vorticity initially contained in $r < r_0$) vorticity field of the rings. The intrusion of a "tentacle" eddy during the merging process as described by Nof (1988) could rensemble both formation of the touching edges of the cloves during the first phase and sliding of the vorticity core intrusions in the second phase. The intrusions in our model are, however, changed by dissipation, which probably prevents the formation of a "padlock" flow as in the Nof (1988) case.

The merging configuration given by Cushman-Roisin (1989) is also represented in our simulations by the arms that eventually detach from the merged vortex. The merging process described here seems to contain all the different merging configurations described in the literature for different models.

In Fig. 12, we show the ΔF_R and F terms in Eq. (14) for the merging and no-merging cases. Here ΔF_T is not shown because it is at smaller amplitude than ΔF_R and F in the central interaction area and it is not very different between the merging and no-merging cases. Furthermore, ΔF_T is at larger scales than ΔF_R and it contributes substantially to the vorticity balance only in the region of the near-field vortices. It is there, in the external field to the central core of the merging rings, that the baroclinic conversion will be strongest as we will see later.

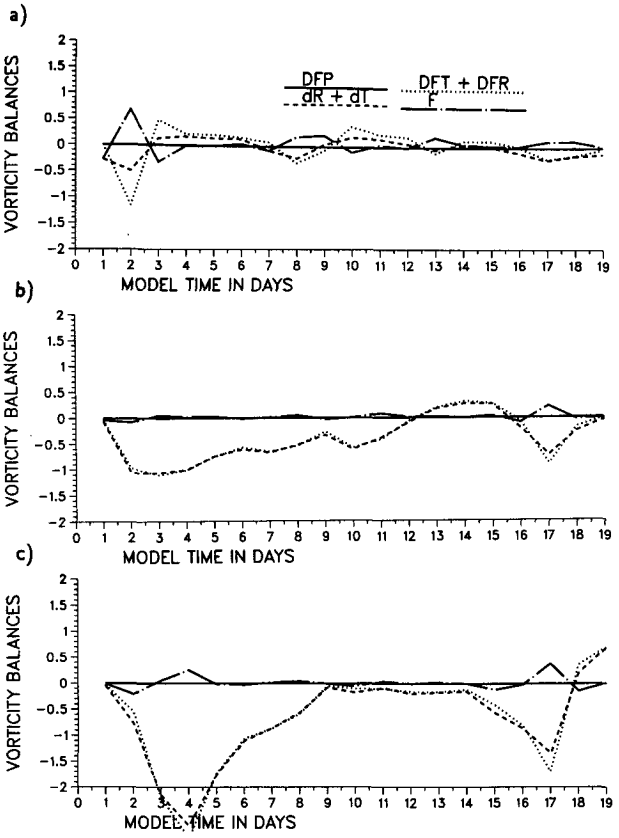

FIG. 13. Integrated vorticity balances at level $z = 300$ m for (a) BG1 case, (b) BC1 case, and (c) BG4 case. Solid line: ΔF_P, dashed line: $\dot{R} + \dot{T}$, dotted line: $\Delta F_T + \Delta F_R$, dash-dot line: F.

At day 1 the principal difference between the merging and no-merging cases is already evident. There is net advection of vorticity in the area of interaction of the vortices, while in the no-merging case ΔF_R and F almost totally balance out. In the merging case the filtering is very active, particularly along the flat sides of the cloves. At day 3 in the no-merging case there is an attempt to form the same ΔF_R and F structure of the day 1 merging case but at much lower amplitude. At days 5 and 7 the ΔF_R positive-sign centers (regions I and II in Fig. 12) indicate the sliding of the vorticity cores intrusion. At day 7 we also see the rising of the filtering activity to complete the diffusive merging of the vorticity contours. From the vorticity balances it is then evident that the first phase of the merging event is triggered by local positive divergence of relative vorticity fluxes in the interacting area of the cloves. Dissipation increases in strength after day 1 to complete the first phase of merging. The second phase corresponds to strong positive relative vorticity flux divergence on the external sides of the sliding cores, on the nose of the vorticity intrusions, and to an ultimate dissipative mixing of vorticity in the interior of the merged vortex.

In Fig. 13, we show the integrated vorticity balances for the various Γ^2 cases. These results show that the

fast merging case ($\Gamma^2 = 0.1$) has the strongest filtering in phase 1 and the shorter time scales. The higher Γ^2 cases show a tighter inviscid balance. The sharp decrease in the $\Delta F_R + \Delta F_T$ term is mainly due to ΔF_T, which decreases faster in the large Γ^2 cases (2.8). This behavior is similar to the no-merging case (not shown)

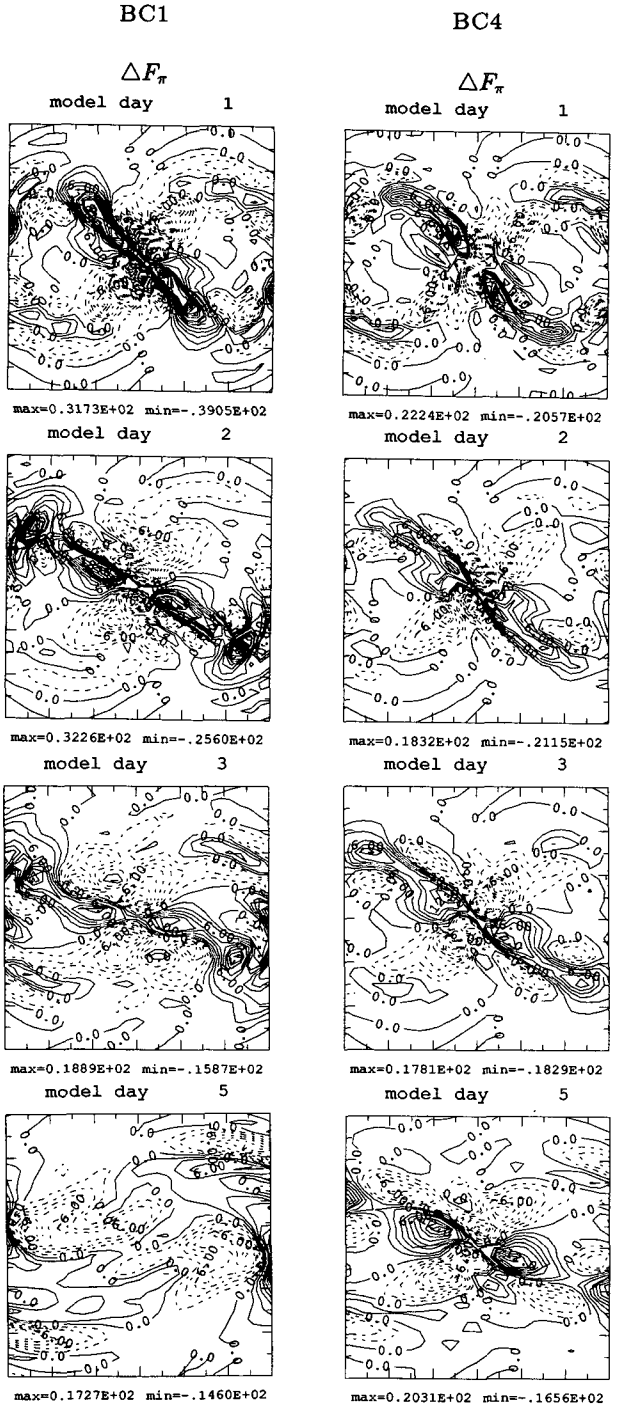

FIG. 14. As in Fig. 10 but for the horizontal divergence of the pressure work term in Eq. (9).

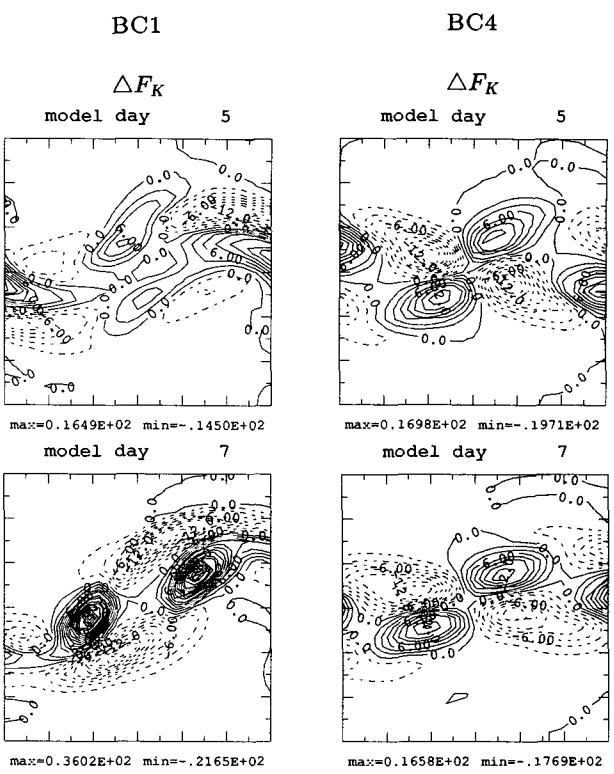

FIG. 15. As in Fig. 10 but for the horizontal divergence of kinetic energy advective fluxes.

and it is retarding the process. In conclusion, from the integrated vorticity balances it is clear that small-scale vorticity is efficiently filtered out in the rapidly merging case with respect to the higher Γ^2 cases. During the first phase in the lowest Γ^2 case the balance is

$$\dot{R} = F + \Delta F_R, \tag{15}$$

while in the largest Γ^2 cases the balance is

$$\dot{R} + \dot{T} = \Delta F_R + \Delta F_T. \tag{16}$$

During the second phase of merging the balance in (16) shows a dominance of the ΔF_T contribution over the ΔF_R.

b. *Energy analysis*

As explained by PR, the presence of a local energy conversion and redistribution between different scales of motion is indicated by the growth of asymmetric poles in the maps of the terms in Eqs. (9) and (11). This growth is intermittent in time and space. When a local "instability" occurs, then a net redistribution and conversion of energy is realized, and it is indicated by the growth of such asymmetries. The quantitative description of baroclinic and/or barotropic energy conversion processes in classical instability problems is shown by PR. Here the reader is reminded that baroclinic instability or direct baroclinic conversion is given

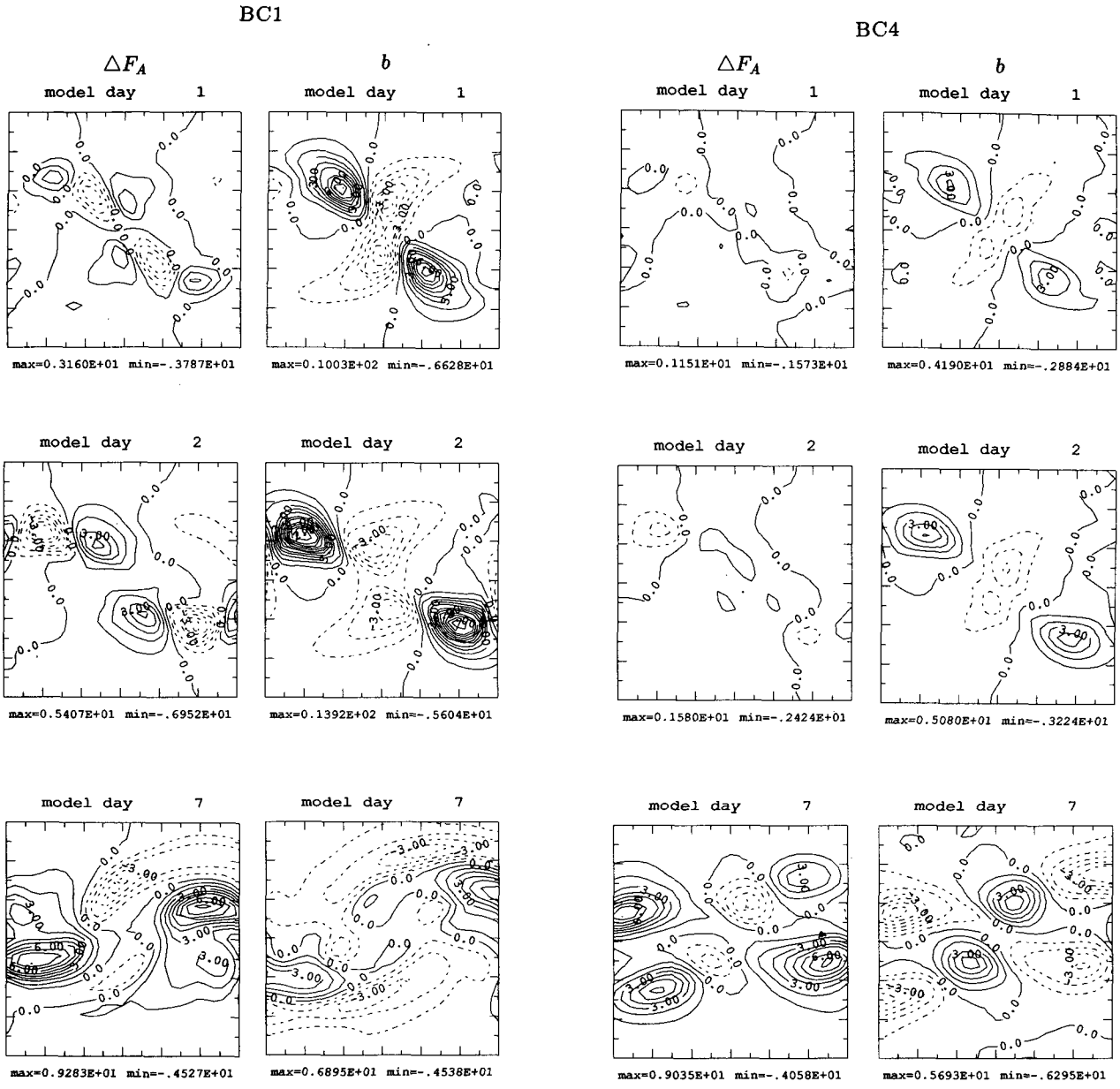

FIG. 16. As in Fig. 10 but for the horizontal divergence of advective fluxes of A and the buoyancy work fields. The contour interval used is equal to one nondimensional unit.

by a net A to K transformation via the b term in Eq. (11). As shown by PR, the barotropic instability is indicated by the growth of asymmetries in the ΔF_π and ΔF_K terms. If the barotropic instability occurs in a baroclinic fluid, K is transformed to A through the b term (also called baroclinic indirect conversion).

In Fig. 14, we show the ΔF_π terms for the merging and no-merging experiments. They show that the first phase of the merging process is associated with a positive net growth of ΔF_π and positive poles along the flat borders of the clove-shaped vortices. This behavior is evident in all the merging experiments and the faster the merging, the sharper is this growth in ΔF_π. In the no-merging case the positive and negative poles of ΔF_π remain about the same size and have about the same relative values in the first three days. Thus, ΔF_π is the term responsible for the energy merging process.

Here ΔF_K is not as important as ΔF_π in the initial phase of merging, but it shows some relevant asymmetries. During the first phase of merging the ΔF_K term has a quadrupolar, almost symmetric, shape in the area of interaction of the vortices. However, it is during the second phase that it becomes very asymmetric, as shown in Fig. 15. At day 7 the differences between the ΔF_K of the merging and no-merging cases are clear. The ΔF_K grows positive poles in the regions of the tip

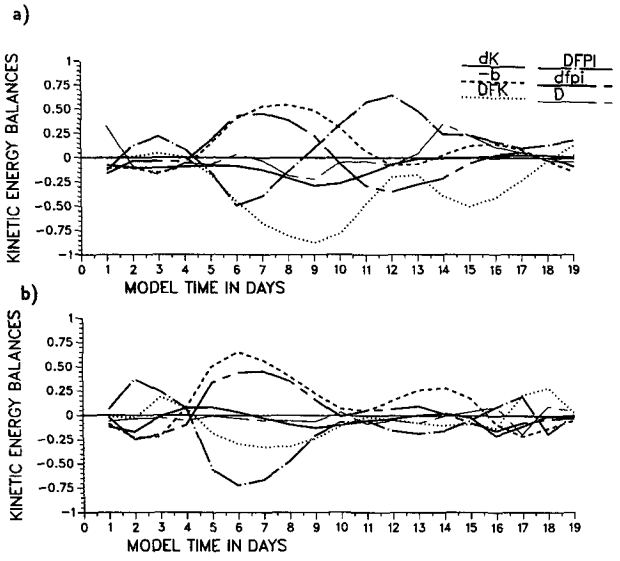

FIG. 17. Integrated energy balances at $z = 300$ m for (a) BC4 case and (b) BC1 case. Solid: $\dot{K}$, dashed: b, dotted: ΔF_K, dash-dot: ΔF_π, thick long-short dash: δf_π, thin long-short dash: D.

of sliding vorticity intrusions, while the no-merging case remains in an unaltered configuration from the start of the process.

Last, we look at the net conversion of K into A by mapping the b and ΔF_A terms. In Fig. 16, we show the ΔF_A and b terms for the merging and no-merging events. In the merging case it is immediately evident that the b term grows the positive poles between day 1 and 2, which gives a net conversion of K into A. The ΔF_A term is generating symmetric poles of positive and negative transport of A. Thus, the net average growth of A in the domain during the first phase of the merging event is due essentially to b and not to ΔF_A. The no-merging case instead shows a much lower amplitude in the terms and no growth of asymmetries at days 1 and 2. At day 3 (not shown) b also starts to grow in the no-merging case but at smaller amplitude.

It is important to point out that the conversion occurs in the region where near-field vortices form in the purely barotropic case. Thus, in the "external field" (region $r > r_0$) there is a net accumulation of A via baroclinic conversion of K. We believe this could be the external field source of energy described by Dewar and Killworth (1990). As shown before, the near-field vortex growth is inhibited in the baroclinic merging. In other words, kinetic energy does not accumulate in the external field, because it is easily converted into A. In the barotropic case this is not possible, and the near-field vortex kinetic energy grows locally due to ΔF_π and ΔF_k processes. However, as shown by Masina and Pinardi (1991), near-field vortices are not essential to the merging process since they can also form in the barotropic no-merging case. Thus, we argue that merging could occur without any "external source" of energy as discussed by Cushman-Roisin (1989). In our case we show that an external-field energy conversion occurs, triggered by the internal vorticity mixing and by a kinetic energy growth due to ΔF_π. We believe this result also supports the Dewar and Killworth (1990) speculations: "Two eddies meet, each possessing significant flows in their exterior. The subsequent interaction results in potential vorticity mixing that can have the effect of altering the momentum distribution in the exterior. This can be consistent with the release of considerable kinetic energy."

During the second phase of merging the b term, in Fig. 16, shows a dominance of negative conversion poles for the BC1 case. On the opposite, the no-merging case forms positive and negative poles of equal amplitude (day 7). This is interpreted as the tendency for the no-merging case to average to zero the net energy conversion in the domain.

To quantify the differences between merging and no-merging cases we show, in Fig. 17, the integrated energy balances. During the first phase of the process (days 1–4), the no-merging case shows a constant b contribution, and the major balance is

$$\dot{K} \approx \Delta F_\pi + D + b. \tag{17}$$

In the merging case it is clear that the balance is

$$\Delta F_K + \Delta F_\pi + \delta F_\pi + b = 0, \tag{18}$$

with almost no filtering contribution. This means that

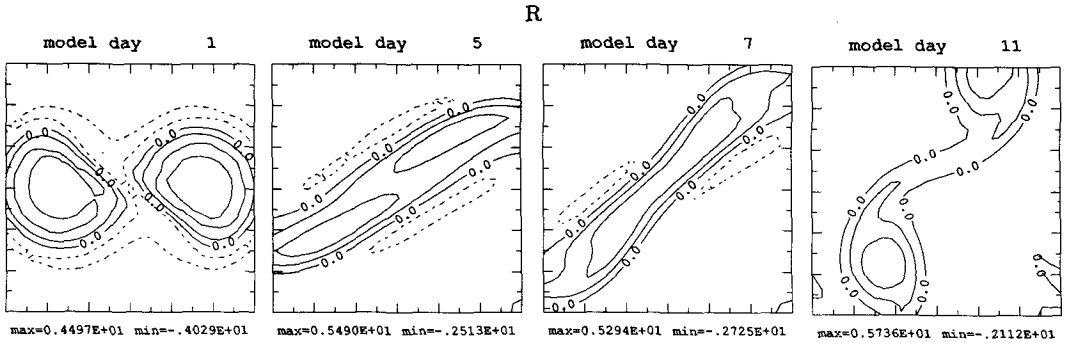

FIG. 18. As in Fig. 11 but for the BG4 experiment.

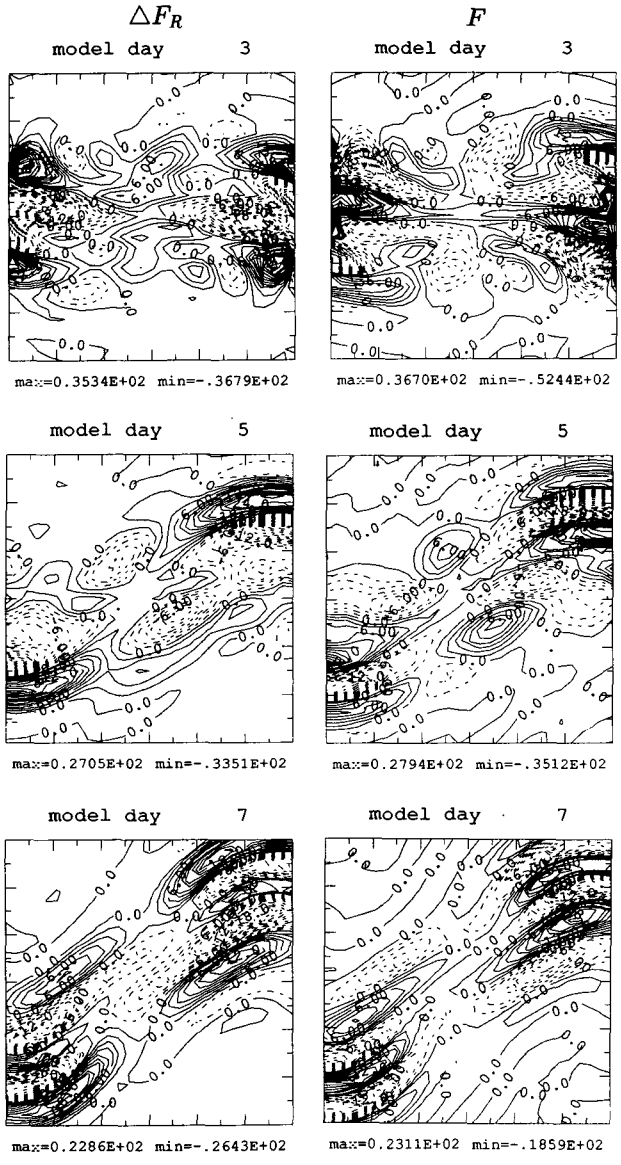

FIG. 19. As in Fig. 12 but for the BG4 case.

during the first phase the ΔF_K and ΔF_π terms redistribute horizontally kinetic energy, which is converted to A and exported vertically to other levels. In the no-merging case, however, the energy redistribution process is mainly dissipated and the small residual is converted to A at a small rate. This process indicates that the triggering of the merging process is given by the growth of asymmetries in the ΔF_K and ΔF_π terms. When the local K redistribution is rapid and is not dissipated as in the no-merging case, the b indirect baroclinic conversion is very efficient in the external field.

c. *EVA of metastable merging*

We now examine the energy and vorticity balances for the metastable cases ($0.2 < \Gamma^2 < 0.7$), and we analyze only the case of $\Gamma^2 = 0.4$ (G4 in Table 2), the intermediate one in the range of Γ^2 values. All other metastable cases are clearly similar. We will outline the differences in energy and vorticity transport and conversion between the central parameter case (BC1) and the metastable case so that the process of splitting the merger vortex can be interpreted.

In Fig. 18, we show the relative vorticity, R, contribution to the potential vorticity, Q. During the first phase of merging (only day 1), the merging proceeds in a similar manner between BC1 and G4, for example, the two initial vortices are shaped like cloves and fuse at their nearest touching borders. At day 5 it is clear that the vorticity core intrusions are sliding one above the other, as at day 7 for the BC1 case of Fig. 10. Here the sliding occurs before that in the BC1 case because the initial phase of merging is faster in the G4 case than in BC1. At day 7 the merging vortex is already splitting. At day 11, what could have been the merger vortex has split totally into two distinct vortices, which have higher values of R than the initially separated vortices of the initial condition.

In Fig. 19, we show the ΔF_R term at three instants for the G4 case. While the BC1 case shows the growth

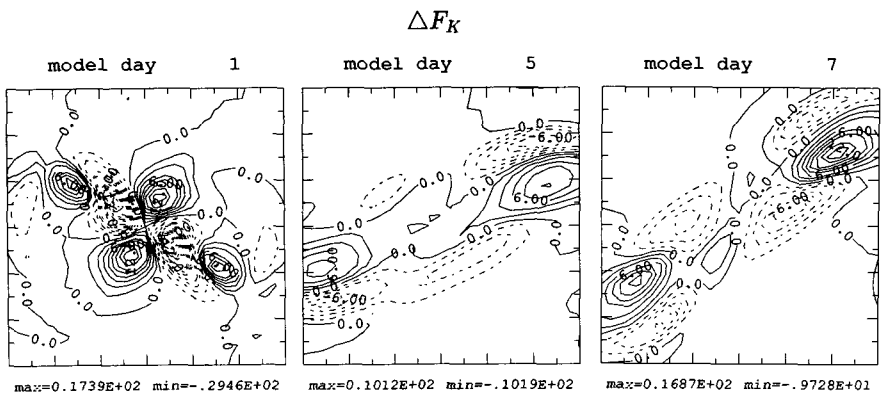

FIG. 20. The horizontal divergence of kinetic energy advective fluxes for the BG4 experiment. The contour interval is two nondimensional units.

of positive poles of advection of relative vorticity in the central merging region (regions I and II in Fig. 12), the G4 case shows the total absence of this signal. Furthermore, the G4 case shows a high correlation between the ΔF_R and the F term, indicating that no net transport or accumulation of vorticity is occurring. Note that the BC1 case shows at day 7 the growth of positive poles of ΔF_R, which are not highly correlated with the filter (see Fig. 12).

To interpret this process of splitting of the merger vortex we have to examine the energy balances. The first outstanding difference between BC1 and G4 energy balances is contained in the behavior of the ΔF_K term in the kinetic energy equation. In Fig. 20, we show the term at three different times inside the G4 experiment. The initial distribution (day 1) of this term is identical to BC1 (not shown); for example, positive and negative almost symmetric poles persist without a relevant growth of asymmetries during the whole first phase of merging. However, during the second phase and in the area of interaction of the vortex core intrusions no positive advection poles of ΔF_K develop between days 5 and 7, contrary to the BC1 case of Fig. 15. Thus, there is no net accumulation of kinetic energy in the region of the sliding vortices due to lack of conversion of A into K, as we can see in Fig. 21. The ΔF_A advection term does not generate positive poles during the first phase, as in the BC1 case (Fig. 16), and it is instead exporting A from the area of the K to A conversion. Consequently during the second phase, the buoyancy work b does not convert A into K in the region of the sliding intrusions. Thus, the process of baroclinic conversion is inhibited in the metastable cases producing a weak interaction of the sliding vorticity core intrusions, which do not fuse stably.

In conclusion, the metastable cases seem to be associated with a weakening of the baroclinic redistribution and conversion processes occurring during the first and second phase of merging. Initially the metastable merging process proceeds normally since it is triggered by a barotropic redistribution mechanism that dominates the energy balances. However, when the second phase of merging starts and the baroclinic terms become partly responsible for the final merging, the ΔF_A exports A from the region and consequently the A to K conversion is weak, if not absent, during the second phase. Thus, the region of $0.2 < \Gamma^2 < 0.7$ does not produce enough baroclinic conversion to make the sliding vorticity core intrusions strongly interactive so as to produce final merging.

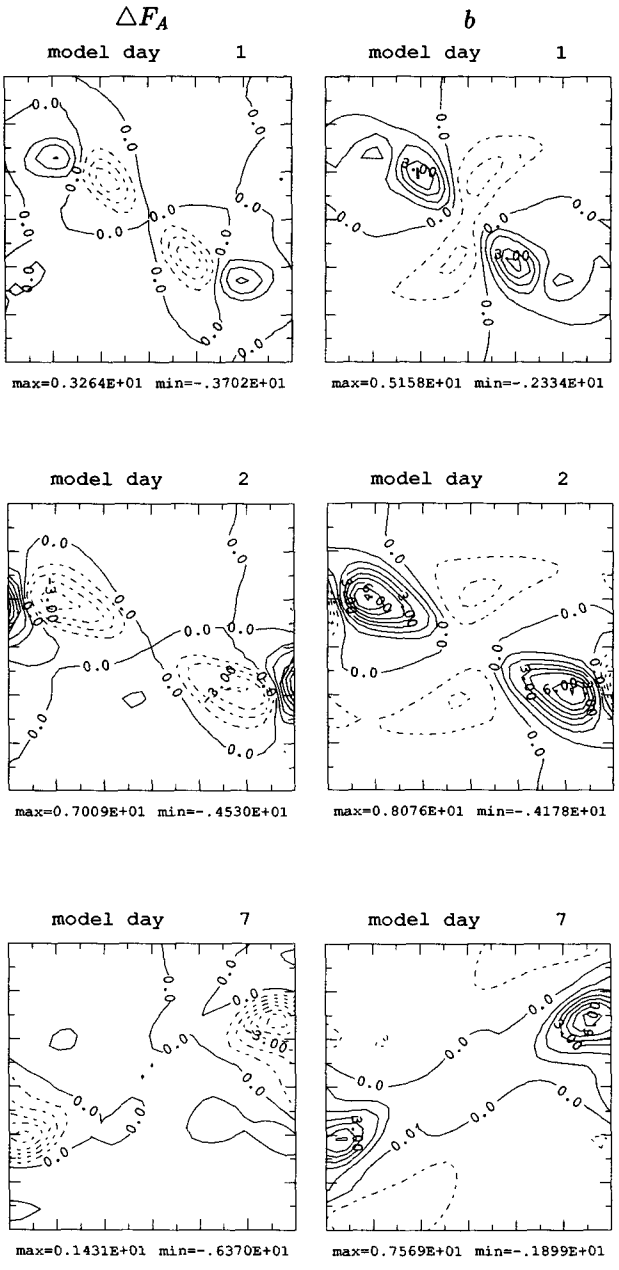

FIG. 21. The horizontal divergence of (a) advective A fluxes and (b) buoyancy work fields for the BG4 experiment. The contour interval is one nondimensional unit.

6. Conclusions

In this study we have simulated and analyzed the merging of axisymmetric baroclinic vortices in a quasigeostrophic model. The stratification and model parameters are typical of the Gulf Stream region, and the initial rings fit the ring structure found by Olson (1980).

The results shown here can be summarized as follows:

- The baroclinic ringlike vortex merger is slower than the purely barotropic process. The barotropic process produces a single vortex merger structure after 5 days while the baroclinic case fuses completely at day 8.

• The fusion process can produce three new isolated structures with respect to the initial condition: a vortex merger, secondary vortices detaching from the filamenting arms, and near-field vortices. Near-field vortices form naturally in totally or highly barotropic systems and they can couple with the secondary vortices forming dipoles. In baroclinic systems near-field vortices are weak if not suppressed. The secondary vortices are strongest in the baroclinic cases and they develop easily into monopoles.

• The merging process is shown to occur in two phases: the first corresponds to the clove shaping of the vorticity front of the vortices and the second consists of the sliding of the remaining vorticity core intrusions. Diffusive mixing of the vorticity cores occurs during both phases, producing the final fusion of the interacting vortices. The fusion seems then to be associated with an "internal" horizontal vorticity redistribution process or mixing.

• The Γ^2 value increase in Eq. (1), corresponding to a smaller first Rossby radius of deformation of the system, produces slower merging during the first phase of merging, but the final result is similar to the standard baroclinic case. We call this mechanism a "saturation" effect that occurs if we decrease the Rossby radius of deformation of the system over a certain limit.

• The Γ^2 value decrease, corresponding to a larger first Rossby radius of deformation of the system, speeds up the process of merging, thus producing an irreducible final distribution of vortices with respect to the higher Γ^2 cases.

• Shallow vortices merge more slowly than deep ones for fixed environmental parameters. There is an almost perfect analogy between the behavior of shallower vortices embedded in a large Rossby radius of deformation environment and deeper vortices surrounded by a small Rossby radius of deformation environment.

• In a baroclinic environment and for fixed initial separation distance of the vortices there is the possibility of a metastable merging; for example, the forming merger vortex splits into two new vortices due to a weaker interaction of the sliding vorticity core intrusions.

• The EVA of the merging process has shown that the triggering mechanism resides in the advection of the relative vorticity term and the growth of asymmetries in the horizontal divergence of the pressure work term. Alternatively, we can say that a horizontal energy redistribution process triggers a baroclinic conversion mechanism of K into A of the initial vortices system. This conversion occurs in the position of the formation of near-field vortices and occurs very rapidly at the beginning of the merging process. The second phase of merging is, instead, triggered by a baroclinic energy conversion of A into K and a horizontal energy transport via ΔF_K, which induces a strong interaction between the sliding cores. Metastable merging occurs because the ΔF_A term depletes the area of A that is not efficiently converted to K during the second phase of merging.

Our study seems to indicate that the process of merging is associated with an "internal" vorticity mixing. This internal vorticity "mixing" corresponds in our model to a horizontal kinetic energy redistribution process, which in turn triggers an inverse baroclinic cascade during the first phase of merging. Hogg and Stommel (1985) and Griffiths and Hopfinger (1987) also speculated that merging should increase the A of the final vortex. In our case we show that the A increase is occurring during the merging process in the region "external" to the initial vorticity cores. The final phase of merging consists of another "internal" mixing process occurring via the sliding of the vorticity core intrusions.

This study shows that the merging can be halted by baroclinic effects. The latter also alter the final merger and secondary vortice configuration with respect to the purely barotropic case. Care should be taken to extrapolate our results directly into the more general framework of PE dynamics as shown by Cushman-Roisin and Tang (1990) for the case of a reduced-gravity model. Future research issues involve the study of these effects in a statistically interacting field of vortices.

Acknowledgments. We are thankful to Dr. Santoro, thesis supervisor, and Dr. Guzzi and Dr. Navarra for their enthusiastic support of this work. This work has been financed by a grant from the Progetto Finalizzato "Calcolo Parallelo."

REFERENCES

Charney, J. G., R. Fjortoft, and J. von Neumann, 1950: Numerical integration of the barotropic vorticity equation. *Tellus,* **2,** 237.

Cresswell, G. R., 1982: The coalescence of two East Australian Current warm-core eddies. *Science,* **215,** 161–164.

Cushman-Roisin, B., 1989: On the role of filamentation in the merging of anticyclonic lenses. *J. Phys. Oceanogr.,* **19,** 253–258.

——, and B. Tang, 1990: Geostrophic turbulence and emergence of eddies beyond the radius of deformation. *J. Phys. Oceanogr.,* **20,** 97–113.

Dewar, W. K., and P. D. Killworth, 1990: On the cylinder collapse problem, mixing, and the merger of isolated eddies. *J. Phys. Oceanogr.,* **20,** 1563–1575.

Gill, A., and R. Griffiths, 1981: Why should two anticyclonic eddies merge? *Ocean Model.,* **41,** 10.

Griffiths, R. W., and E. J. Hopfinger, 1986: Experiments with baroclinic vortex pairs in a rotating fluid. *J. Fluid Mech,* **173,** 501–518.

——, and ——, 1987: Coalescing of geostrophic vortices. *J. Fluid Mech.,* **178,** 73–97.

Haidvogel, D. B., A. R. Robinson, and E. E. Schulman, 1980: The accuracy, efficiency, and stability of three numerical models with application to open ocean problems. *J. Comput. Phys.,* **34,** 1–53.

Hogg, N. G., and H. M. Stommel, 1985: The heton, an elementary interaction between discrete baroclinic-geostrophic vortices and its implication concerning eddy heat flow. *Proc. R. Soc. London,* **A397,** 1–20.

McGillicuddy, D. J., 1987: Quasigeostrophic modelling of isolated

vortices. B. A. thesis, Department of Engineering Sciences, Harvard University.

McWilliams, J. C., and N.J. Zabusky, 1982: Interaction of isolated vortices. I: Modons colliding with modons. *Geophys. Astrophys. Fluid Dyn.*, **19,** 207–227.

Masina, S., and N. Pinardi, 1991: Merging of barotropic symmetric vortices: A case study for Gulf Stream rings. *Il Nuovo Cimento,* **14C**(6), 539–553C.

Melander, M. V., N. J. Zabusky, and J. C. McWilliams, 1987: Axisymmetrization and vorticity-gradient intensification of an isolated two-dimensional vortex through filamentation. *J. Fluid Mech.*, **178,** 137–159.

——, ——, and ——, 1988: Symmetric vortex merger in two dimensions: Causes and conditions. *J. Fluid Mech.*, **195,** 303–340.

Miller, R. N., A. R. Robinson, and D. B. Haidvogel, 1983: A baroclinic quasi-geostrophic open-ocean model. *J. Comp. Phys.*, **50,** 38–70.

Nof, D., 1988: The fusion of isolated nonlinear eddies. *J. Phys. Oceanogr.*, **18,** 887–905.

——, and L. M. Simon, 1987: Laboratory experiments on the merging of nonlinear anticyclonic eddies. *J. Phys. Oceanogr.*, **17,** 343–357.

Olson, D. B., 1980: The physical oceanography of two rings observed during the cyclonic rings experiment. Part II: Dynamics. *J. Phys. Oceanogr.*, **10,** 514–528.

Overman, E. A., and N. J. Zabusky, 1982: Evolution and merger of isolated vortex structures. *Phys. of Fluids,* **25,** 1297–1305.

Pavia, E. G., and B. Cushman-Roisin, 1990: Merging of frontal eddies. *J. Phys. Oceanogr.*, **20,** 1886–1906.

Pinardi, N., and A. R. Robinson, 1986: Quasigeostrophic energetics of open ocean regions. *Dyn. Atmos. Oceans,* **10,** 185–219.

——, and R. F. Milliff, 1989: A note on consistent quasi-geostrophic boundary conditions in partially open, simply and multiply connected domains. *Dyn. Atmos. Oceans,* **14,** 65–76.

Polvani, L. M., N. J. Zabusky, and G. R. Flierl, 1989: Two-layer geostrophic vortex dynamics. Part 1: Upper-layer V-states and merger. *J. Fluid Mech.*, **205,** 215–242.

Rhines, P. B., 1977: The dynamics of unsteady currents. *The Sea,* Vol. 6, Wiley & Sons, 189–318.

——, 1979: Geostrophic turbulence. *Ann. Rev. Fluid Mech.*, **11,** 401–41.

Robinson, A. R., and L. J. Walstad, 1987: The Harvard open-ocean model: Calibration and application to dynamical process, forecasting, and data assimilation studies. *J. Appl. Numer. Math.*, **3,** 89–131.

——, M. A. Spall, and N. Pinardi, 1988: Gulf Stream simulation and the dynamics of ring and meander processes. *J. Phys. Oceanogr.*, **18,** 1811–1853.

——, J. A. Carton, N. Pinardi, and C. N. K. Mooers, 1986: Dynamical forecasting and dynamical interpolation: An experiment in the California Current. *J. Phys. Oceanogr.*, **16,** 1561–1579.

Shapiro, R., 1970: Smoothing, filtering and boundary effects. *Rev. Geophys. Space Phys.*, **2,** 491–507.

——, 1971: The use of linear filtering as a parameterization for atmospheric diffusion. *J. Atmos. Sci.*, **28,** 523–531.

Verron, J., E. J. Hopfinger, and J. C. McWilliams, 1990: Sensitivity to initial conditions in the merging of two-layer baroclinic vortices. *Phys. Fluids A,* **2**(6), 886–889.